GEOPHYSICAL RESEARCH LETTERS, VOL. 28, NO. 24, PAGES 4619-4622, DECEMBER 15, 2001

Ageostrophic transport in the upper layers of the tropical Atlantic Ocean

Silvia L. Garzoli and Robert L. Molinari

NOAA/Atlantic Oceanographic and Meteorological Laboratory, Miami, Florida

Abstract. A test of the theoretical Ekman relation in the tropical Atlantic Ocean is performed by comparing estimated Ekman transport with observations collected along two transects symmetric about equator (6°N and 6°S). Ekman transport is calculated theoretically using ship winds and climatological data. Total ageostrophic transport is obtained by subtracting the observed geostrophic transports from the measured total transports using the data collected along the two transects. Along 6°S, both the zonal mean ageostrophic transport and it's variability with longitude can be accounted for by the theoretical Ekman transport. Along 6°N, the total ageostrophic and Ekman transports agree, but significant differences are found in the cumulative transport curves between the African coast and about 40°W. These departures from theory may be related to the effect of advective terms in the Ekman relation and/or other ageostrophic motion at the reference depth for the comparisons. Begin typing abstract here.

Introduction

The Acoustic Doppler Current Profiler (ADCP) provides a mechanism for directly observing total upper water column transport. When combined with calculations of geostrophic transport from Conductivity, Temperature and depth (CTD) observations, estimates of the ageostrophic component of transport are possible. The theoretical Ekman component of the total ageostrophic flow can be derived from different wind products to determine the contribution of the former to the latter. *Chereskin and Roemmich* [1991], *Wijffels et al.* [1994], and *Chereskin et al.* [1997] have compared directly measured ageostrophic and theoretical Ekman transports in the tropical oceans. Results are summarized in Table 1. Except for the Pacific sections, the differences between theory and observations are typically less than 5 Sv. In addition, *Chereskin and Roemmich* [1991] and *Wijffels et al.* [1994] show cumulative curves relative to longitude of theoretical and observed ageostrophic transports. The forms of the two curves are very similar in both studies. During July and August 1997, the R/V *Seward Johnson* completed two basin-wide transects along 6°N and 6°S in the tropical Atlantic. Herein, we follow *Chereskin and Roemmich* [1991] to compute estimates of the ageostrophic components of velocity along 6°S and 6°N. These estimates are compared to those derived from theoretical Ekman computations. The main difference between the present calculations and those referenced above is that they are made considerably closer and symmetric to the equator.

Paper number 2001GL013473.

Data Collection and Calibration

Note Data were collected along 6°N between July 7-15, 1997 and along 6°S from July 30-August 10, 1997. Most of the CTD/LADCP casts were taken to a depth of 2000 m depth. Typical station spacing was 110 km along 6°N and 160 to 275 km along 6°S, with closer spacing near shore. A Seabird model 911 plus CTD was calibrated by bottle measurements of salinity using processing software provided by the manufacturer (*Fleurant et al.*, [2000]). The LADCP data are not used because of their similarity to the shipboard ADCP (SADCP) measurements within the upper 300m (i.e., average difference between the two was 0.02 m/s). Data from the RD Instruments 150 kHz SADCP were acquired with a blanking interval of 4 m, vertical pulse length of 16 m, and vertical bin size of 8 m. They were stored as 1.5minute averages. P-code GPS navigation, pitch and roll measurements from the ship's gyrocompass, and directional GPS data were logged for use in processing of the SADCP measurements. These data are used to correct for off sets in transducer orientation relative to the ships centerline. After being corrected for ship motion, the SADCP data were further averaged to 15 a final product with a resolution of 15 minutes in time and 8 m in depth. The *Seward Johnson's* meteorological system logged hourly ship speed and direction and relative wind measurements from a Bendix anemometer mounted on the ship's mast approximately 17 m above waterline. These measurements were converted to zonal and meridional components of the wind at 10-m height. Climatological data from *Hellerman and Rosenstein* [HR, 1983] were compared to the ship data to determine the representativeness of the 1997 wind fields.

Methodology for Transport Calculations

Average vertical profiles of meridional velocity were estimated between stations from the SADCP, excluding on station data. Velocity profiles relative to the mean velocity between 100 and 150 m were then obtained. For these calculations, the assumption is made that the total velocity at 150 m is in geostrophic balance (i.e., the ageostrophic velocity is limited to the shallower depths, *Chereskin and Roemmich*, [1991]). Geostrophic velocity profiles were computed between station pairs, from the CTD casts also relative to 150 m. Transport estimates between station pairs were obtained from the vertically integrated velocities ($\int vdz$) and the cumulative transport along the section by integration from the eastern boundary. Errors in the total transports were calculated following *Chereskin and Roemmich* [1991]. The uncertainty in SADCP transport between station pairs is 0.6 Sv. The cumulative error along the sections is 1.5 Sv. Estimates of Ekman transport were computed using observed and climatological winds. Calculations follow those of *Chereskin and Roemmich* [1991] and *Chereskin et al.* [1997]. To

Table 1. Ekman transports calculated using observed winds from this study from SADCP and climatological winds from HR (1983). Column 3: total ageostrophic transport. Column 4: absolute difference between columns (1) and (3). All units are Sverdrups ($1Sv=10^6$ m^3/s).

	Ekman transport Ship Winds	Ekman transport Climatology (HR)	Ageostrophic Transport	Absolute Difference between columns 1 and 3
	(1)	(2)	(3)	(4)
Chereskin and Roemmich [1991]				
11°N/Atlantic/March 1989	8.8 ± 0.13	13.5 ± 0.3	12.0 ± 5.5	3.2
Wijffels et al. [1994]				
10°N/Pacific/February-May 1989	52.5 ± 10	67.8 ± 20	61.8 ± 10	9.3
Chereskin et al. [1997]				
8.5°N/Indian/June 1995	-19.1 ± 3.8	-22.7 ± 4.5	-17.6 ± 2.4	1.5
8.5°N/Indian/September 1995	-6.4 ± 1.3	-9.6 ± 1.9	-7.9 ± 2.7	1.5
This study				
6°S/Atlantic/August 1997	-11.2 ± 1.4	-20.4 ± 6.1	-16.2 ± 2.5	5.0
6°N/Atlantic/July 1997	1.8 ± 0.9	3.2 ± 1.0	0.8 ± 2.5	1.0

compute the Ekman transport from the ship winds, the zonal wind stress (τ_x) for each station pair was computed using:

$$\tau_x = C_D \rho_{air} u|\bar{u}| \quad (1)$$

where ρ_{air} air density is 1.29 kg/m^3, u is the average zonal wind component $\bar{u}$, and the vector wind between each station pair and C_D is the drag coefficient from *Large and Pond* [1981]. This formulation assumes a neutrally stable atmosphere and a C_D dependent on wind speed. Ekman transport M_y, was then computed for each station pair using:

$$M_y = -\tau_x \Delta_x / f\rho_{water} \quad (2)$$

where Δx is the projected distance (distance along a line of constant latitude) between the two stations, f is the Coriolis parameter at the average latitude of the two stations, and ρ_{water} the density of water is 1025 kg/m^3. Errors in the winds calculated from the ship sensors are caused by two sources: the inherent error of the anemometer and the error caused by the ship motion. Again, following *Chereskin and Roemmich* [1991] the uncertainties in Ekman transport derived from these wind observations are 0.9 Sv and 1.4 Sv at 6°N and 6°S respectively. Uncertainty in the estimates of drag coefficient causes another error in Ekman transport. This is estimated to be 25% *(Large and Pond,* 1981). It is assumed that the *Hellerman and Rosenstein* [1983] products overestimate the wind stress by 30% *(Harrison,* 1989). This value was used as the error on the Ekman transports derived from the climatology.

Results

Table 1 gives the cumulative theoretical Ekman transport estimates obtained from both the synoptic ship and climatological winds, and the ageostrophic transports. Results are compared with previous estimates.

Along 6°S, the zonally integrated or cumulative Ekman transport calculated from HR climatological winds (-11.2± 1.4 Sv) is statistically larger than those calculated from the ship winds (-20.4±6.1 Sv). Along 6°N, the cumulative transport calculated from the July synoptic and climatological winds (1.8±0.9 and 3.2±1.0 Sv respectively) are very similar. Column 3 of Table 1, shows the cumulative ageostrophic transport obtained as a difference between the total transport measured with the ADCP and the geostrophic transport from the CTD data. The difference between the total ageostrophic transport and the estimated Ekman transports (column 4), are similar to the differences found in earlier studies. In isolation, these similarities would suggest that the main contribution to ageostrophy is the Ekman transport. However, a closer look at the cumulative transport curves along both sections (Figure 1) indicates that this is not the case.

Along 6°S (Figure 1, bottom panel), with the exception of an increase in the ageostrophic transport between 0° and 4°E, theoretical and observed estimates show a southward transport increasing monotonically from the eastern boundary. The Ekman transport obtained from climatological winds is statistically similar, to the observed ageostrophic transport. However, close to the western boundary the Ekman transport obtained from the ship winds have a smaller westerly component than climatology resulting in a smaller total integrated transport (11.2±1.4 Sv) than from ageostrophy (-16.2± 2.5 Sv). Along 6°N the total cumulative transport calculated from the ship winds (1.8±0.9 Sv), from HR climatology (3.2±1.0 Sv) and from the observations (0.8± 2.5Sv) are statistically the same (Table 1). Even though the final results agreed, there are significant differences between the theoretical cumulative transport curves calculated from the wind products (Ekman transport) and the ageostrophic transport obtained from the observations (Fig.1, upper panel). The magnitude of the southward ageostrophic flow observed between 12° and 35°W is much larger than the theoretical ones The same analysis was repeated using a 300 m reference level (not shown). Results did not improve. The vertical profile of the transport per unit depth was calculated along both transects. Across the 6°S section, (Figure 2), it has a shape characteristic of the Ekman profile: a surface intensified flow confined in the upper 50 meters, and near zero current below. The net transport per unit depth profile for the section along 6°N (Fig. 2) has a vertical distribution of transport with a minimum in northward transport near 50 m and thus is unlikely to be due only to effect of the wind stress in the surface layer. The data collected during these two transects allow an additional calculation of the divergence of the wind at

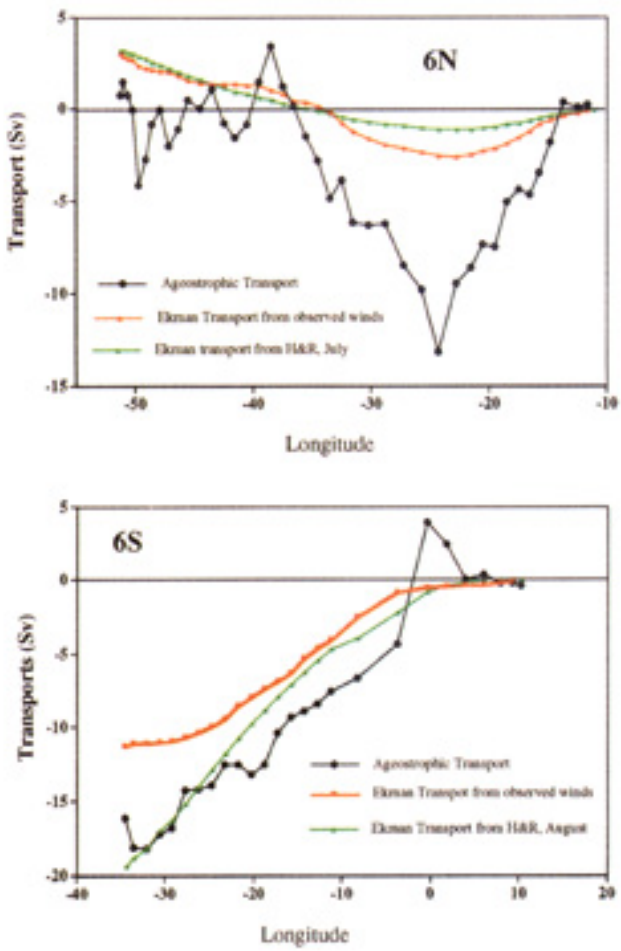

Figure 1. Cumulative sum of the Ekman transport as a function of longitude calculated from the different wind products and the ageostrophic transport from direct observations as a function of longitude along 6°N (upper panel) and 6°S (lower panel).

the equator ($|My^{6S}| + |My^{6N}|$). The divergence of the winds calculated from the HR climatology is 24 Sv ± 7 Sv (Table 1), a value statistically similar to the one obtained by Roemmich (1983) for calculations between 8°N and 8°S: 26.0 ± 5.0 Sv. The divergence of the winds measured during the two transects is smaller, 13 ± 2.3 Sv.

Discussion

Along 6°S, the cumulative Ekman and ageostrophic transports present the same characteristics. The cumulative curves of each variable have the same tendency (Fig. 1) and the total cumulative values of transport are within the limit of the errors (Table1). Finally, the section average velocity profile has the characteristic shape of Ekman transport (Fig. 2).

Thus, we conclude that along 6°S, the ageostrophic transport is primarily Ekman. Along 6°N, the total cumulative Ekman and ageostrophic transports are also similar within the limits of the errors (Table 1). However, the cumulative curves are different in magnitude east of 35°W and in magnitude and direction west of 35°W (Fig. 1). The average transport profile has more vertical structure than a typical Ekman response (Fig. 2). Thus, along this section, the ageostrophic flow is not only due to the Ekman effect. Several candidates other than Ekman were examined for possible contributions to the total ageostrophic flow along 6°N. Sections of the meridional components of the velocity from the SADCP (Figure 3) show that the currents are intensified along the western boundary and are indicative of the North Brazil Current (NBC).

Bands of strong currents with alternating direction are also found offshore of the NBC on the northern section. The bands are most likely representative of the retroflection of the NBC and a meander in the North Equatorial Countercurrent (NECC) observed to the east (Cochrane et al., 1979; Boules et al., 1999). In the central basin, alternating regions of southward and northward total flow are observed. The zonal component of velocity from the 6°N section (not shown) indicates that throughout the section the surface velocities range from 0.50 to 1.00 m/s. This is an indication that the 6°N section was taken close to the axis of the North Equatorial Countercurrent. The presence of these strong inertial currents can explain the discrepancy between theoretical and observed ageostrophic transports west of 35°W The alternating bands of meridional velocity (Figure 3) are also characteristic of Tropical Instability Waves (TIW). The TIW appear in boreal summer in the shear zone between the NECCand South Equatorial Current (SEC), have horizontal length scales of about 1000 km, and have a circular velocity structure at the surface (Hansen and Paul, 1984 and Weisberg and Weingartner, 1988, for example.) However, earlier studies have found these features to be in approximate geostrophic balance. A qualitative consideration of the terms in the horizontal equation of motion using data obtained during the 6°N occupation supports this finding. The vertical sections of the ageostrophic velocities are also shown in Figure 3. They reflect the structures described above. Along 6°S, a circulation flow is observed centered at 0°E, where the larger discrepancy is observed in the cumulative curve as a

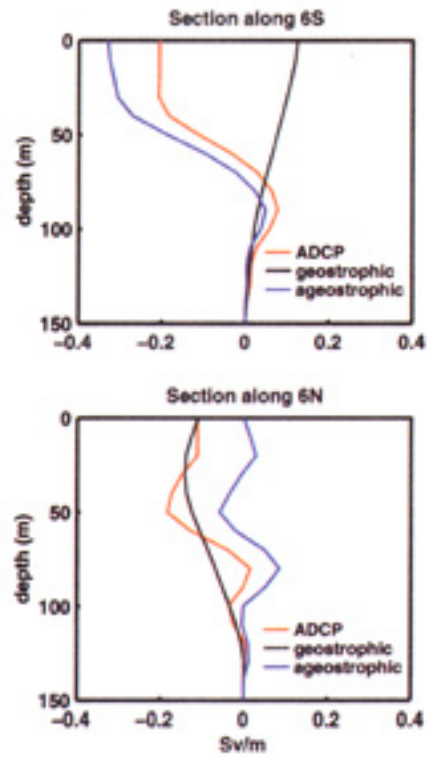

Figure 2. Net total (red), geostrophic (black), and ageostrophic (blue) transport per unit depth. The curves represent a summed profile across 6°S for 150 (lower panel) and 6°N (upper panel).

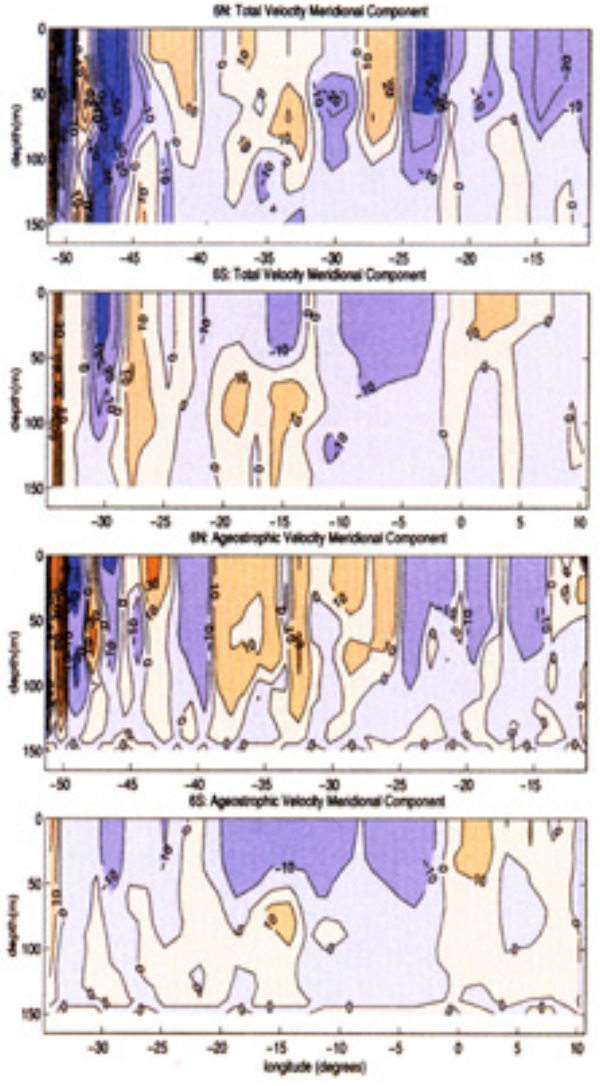

Figure 3. Vertical sections of meridional velocitiy (cm/sec) for the upper 150 m (top panels) and ageostrophic velocities (cm/sec) referenced to 150 m (lower panel) as a function of longitude.

function of latitude (Fig. 1, bottom panel). The meridional velocity section provides the basis for another possible ageostrophic component. East of 25°W the flow is predominantly southward and west of 25°W, predominantly northward. In addition, the horizontal shear between the NECC and the westward SEC is positive, suggesting that the $\partial u/\partial y$ term in the equations of motions could contribute to the transport in the direction of the ageostrophic flow along 6°N. Weisberg and Weingartner [1988] estimated a mean zonal shear profile for the equatorial currents, with the core of the NECC at 6°N (speed 0.6 m/s) and the core of the northern branch of the SEC at 2°N (speed -0.2 m/s). Computing the $v\partial u/\partial y$ term from these estimates and using 0.05 m/s as a mean meridional speed (Figure 1), the $v\partial u/\partial y$ term has the same order of magnitude (1×10^{7} m/s^2) as the wind forcing term. Thus, adding the transport associated with the advective term to the Ekman transport would result in a cumulative transport at 25°W of approximately -5 Sv, leaving about -10 Sv of unexplained ageostrophic transport (Fig. 3). Finally, the possibility that the flow at 150 m along 6°N is not geostrophic and thus can add to the total ageostrophic transport must be considered. An ageostrophic current of only 0.05 m/s at 150 m extending from 15°W to 25°W would result in an ageostrophic transport of 8 Sv in the upper 150 m. However, the data provide no indication of a coherent ageostrophic flow at 150 m that would add sufficient negative ageostrophic transport between 15°W and 25°W and positive transport between 25°W and 38°W to account for the discrepancy between the Ekman and total ageostrophic transports shown in Figure 1. Thus, we are presently unable to identify the additional ageostrophic current component at 6°N. Furthermore, because we cannot identify this component we cannot say if the fact that the southward and northward components of ageostrophy approximately are compensated is fortuitous or dynamically driven. On the contrary, along 6°S, this new set of observations lead us to conclude that the ageostrophic transport is wind driven.

Acknowledgments. The authors wish to acknowledge the outstanding effort of the officers and crew of the R/V SEWARD JOHNSON. We also thank Dr. M. Baringer for serving as chief scientist during the occupation of the 6°N section. Roberta Lusic prepared the manuscript for publication. This work was supported in part by NOAA's Office of Global Programs and the Atlantic Oceanographic and Meteorological Laboratory. Insert text here.

References

Boules, B., R.L. Molinari, E. Johns, W.D. Wilson, and K.D. Leaman, Upper layer currents in the western tropical North Atlantic (1989-1991), *J. Geophys. Res.*, 104 (C1), 1361-1376, 1999.

Chereskin, T.K., and D. Roemmich, A comparison of measured and wind-derived Ekman transport at 11°N in the Atlantic Ocean, *J. Phys. Oceanogr.*, 21 (6), 869-878, 1991.

Chereskin, T.K., W.D. Wilson, H.L. Bryden, A. Ffield, and J. Morrison, Observations of the Ekman balance at 8°30'N in the Arabian Sea during the 1995 southwest monsoon, *Geophys. Res. Lett.*, 24 (21), 2541-2544, 1997.

Cochrane, J.D., F.S. Kelly, and C.D. Oiling, Subthermocline countercurrents in the western equatorial Atlantic Ocean, *J. Phys. Oceanogr.*, 9 (4), 724-738, 1979.

Fleurant, C.I., W.D. Wilson, W. E. Johns, S.L. Garzoli, R.H. Smith, D. Fratantoni, P. Richardson, and G.J. Goni, CTD/O_2, LADCP, and XBT measurements collected aboard the *Seward Johnson*, November-December 1998: North Brazil Current Rings Experiment cruise, NOAA Data Report, OAR-AOML 39, 274 pp., 2000.

Hansen, D.V., and C.A. Paul, Genesis and effects of long waves in the equatorial Pacific, *J. Geophys. Res.*, 89, 10,431-10,440, 1984.

Harrison, D.E., On climatological monthly mean wind stress and wind stress curl field over the World Ocean, *J. Climate*, 2 (1), 57-70, 1989.

Hellerman, S., and M. Rosenstein, Normal monthly wind stress over the World Ocean with error estimates, *J. Phys. Oceanogr.*, 13 (7), 1093-1104, 1983.

Large, W.G., and S. Pond, Open ocean momentum flux measurements in moderate to strong winds, *J. Phys. Oceanogr.*, 11 (3), 324-336, 1981.

Weisberg, R.H., and T.J. Weingartner, Instability waves in the equatorial Atlantic Ocean, *J. Phys. Oceanogr.*, 18 (11), 1641-1657, 1988.

Wijffels, S., E. Firing, and H. Bryden, Direct observations of the Ekman balance at 10°N in the Pacific, *J. Phys. Oceanogr.*, 24 (7), 1666-1679, 1994.

Silvia L. Garzoli, NOAA/AOML, 4301 Rickenbacker Causeway, Miami, Florida 33149 (e-mail: Silvia.Garzoli@noaa.gov).

(Received May 18,200; revised August 31, 2001; accepted September 19, 2001.)